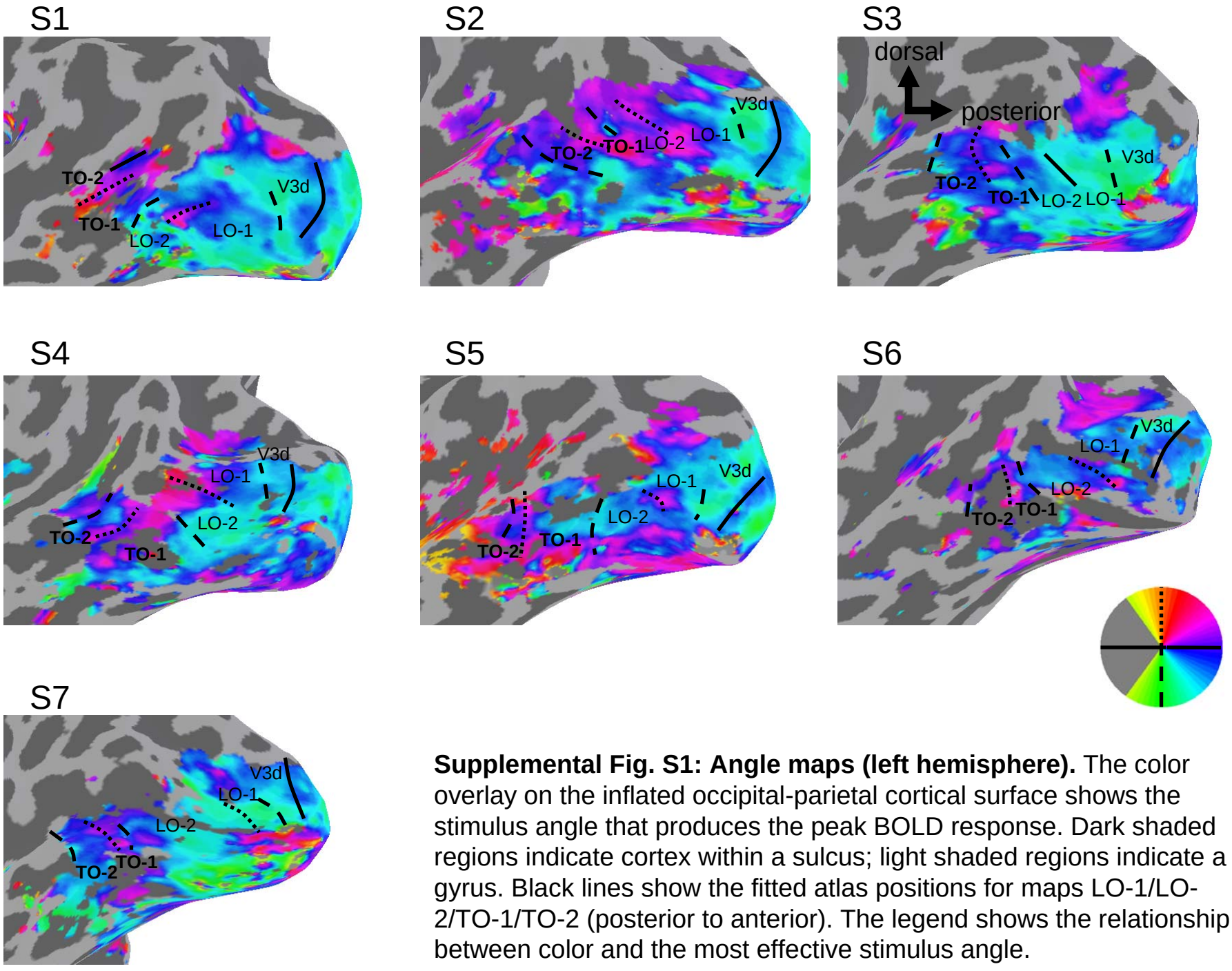

Supplemental Fig. S1: Angle maps (left hemisphere). The color overlay on the inflated occipital-parietal cortical surface shows the stimulus angle that produces the peak BOLD response. Dark shaded regions indicate cortex within a sulcus; light shaded regions indicate a gyrus. Black lines show the fitted atlas positions for maps LO-1/LO-2/TO-1/TO-2 (posterior to anterior). The legend shows the relationship between color and the most effective stimulus angle.

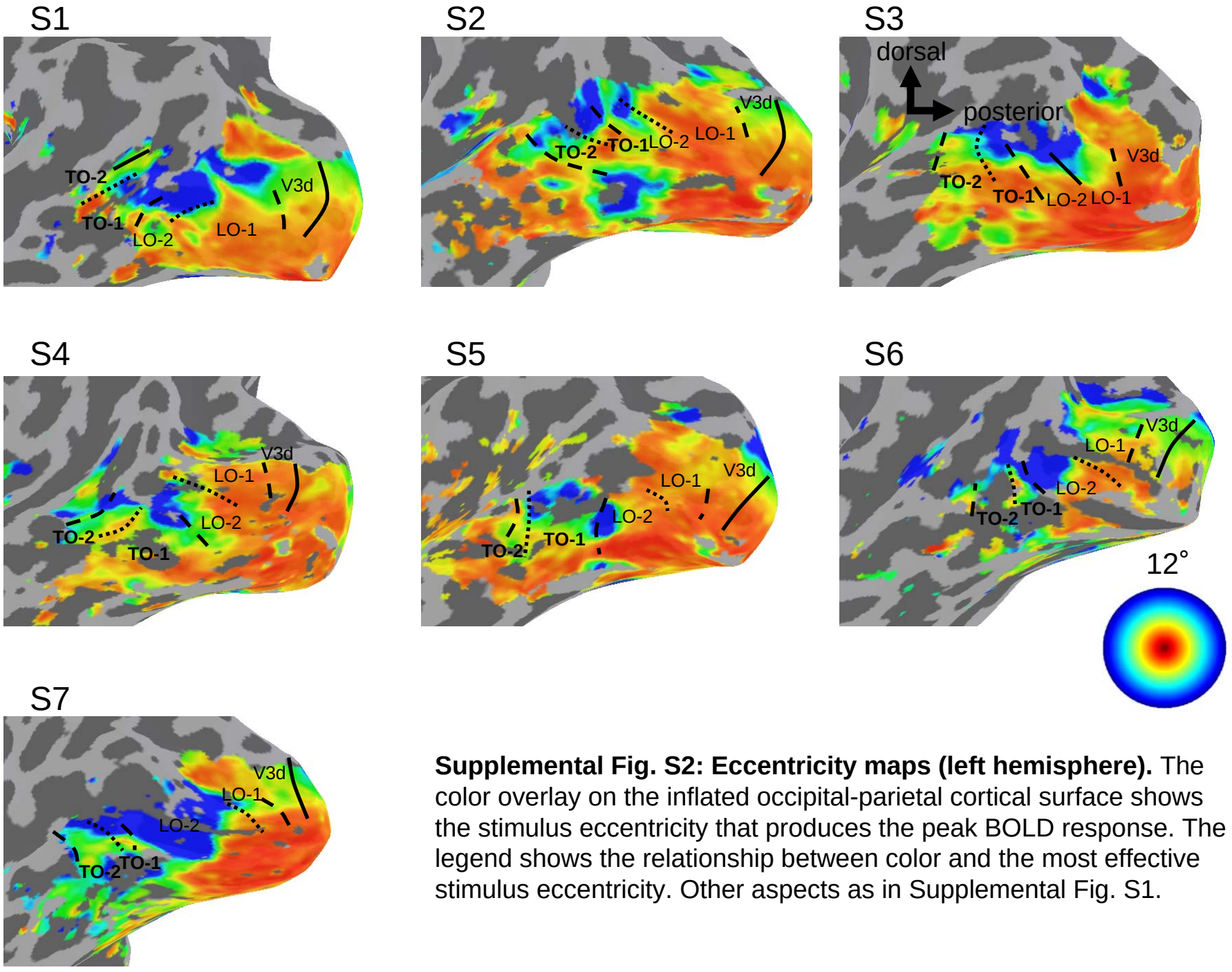

Supplemental Fig. S2: Eccentricity maps (left hemisphere). The color overlay on the inflated occipital-parietal cortical surface shows the stimulus eccentricity that produces the peak BOLD response. The legend shows the relationship between color and the most effective stimulus eccentricity. Other aspects as in Supplemental Fig. S1.

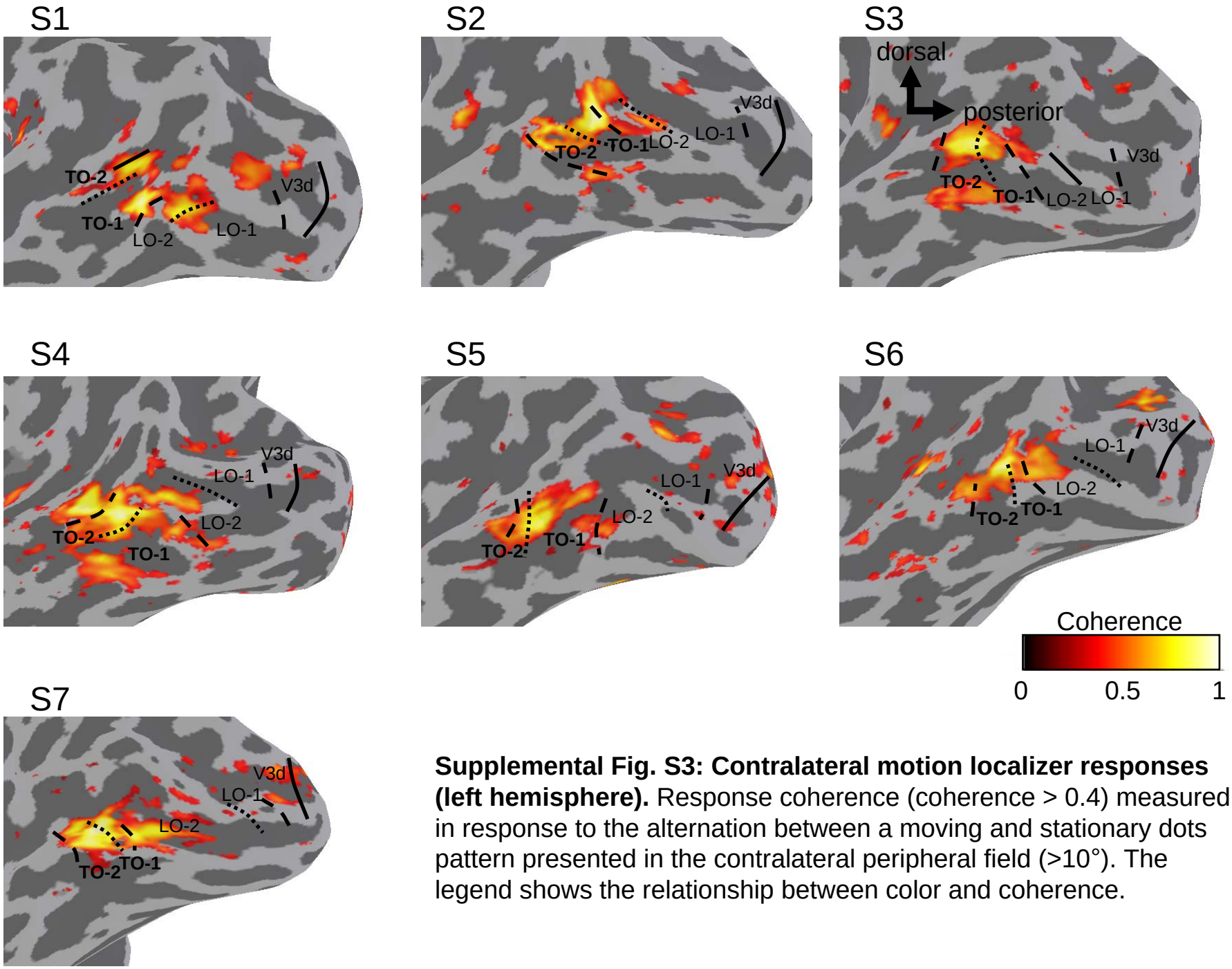

Supplemental Fig. S3: Contralateral motion localizer responses (left hemisphere). Response coherence (coherence > 0.4) measured in response to the alternation between a moving and stationary dots pattern presented in the contralateral peripheral field (>10°). The legend shows the relationship between color and coherence.

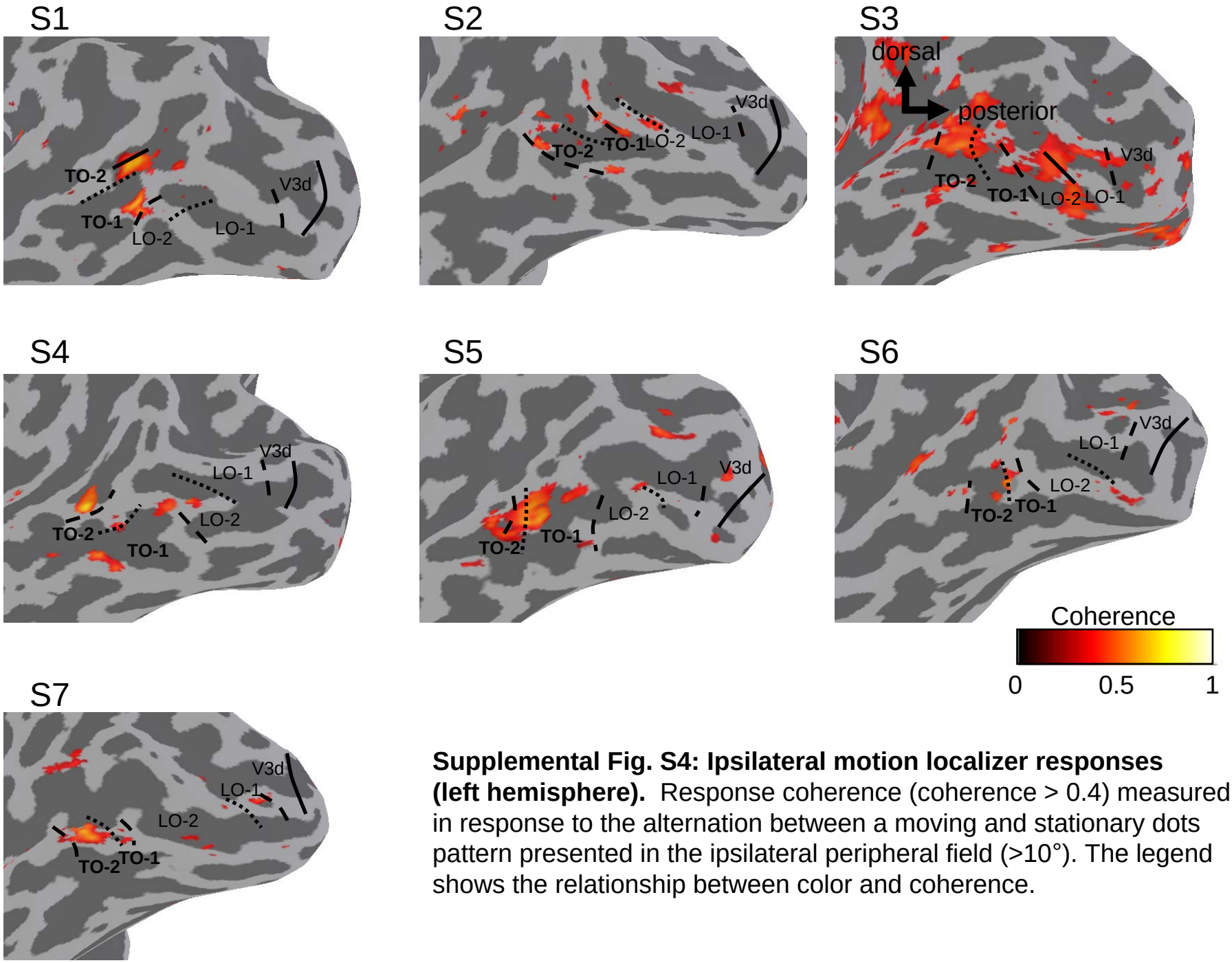

Supplemental Fig. S4: Ipsilateral motion localizer responses (left hemisphere). Response coherence (coherence > 0.4) measured in response to the alternation between a moving and stationary dots pattern presented in the ipsilateral peripheral field (>10°). The legend shows the relationship between color and coherence.

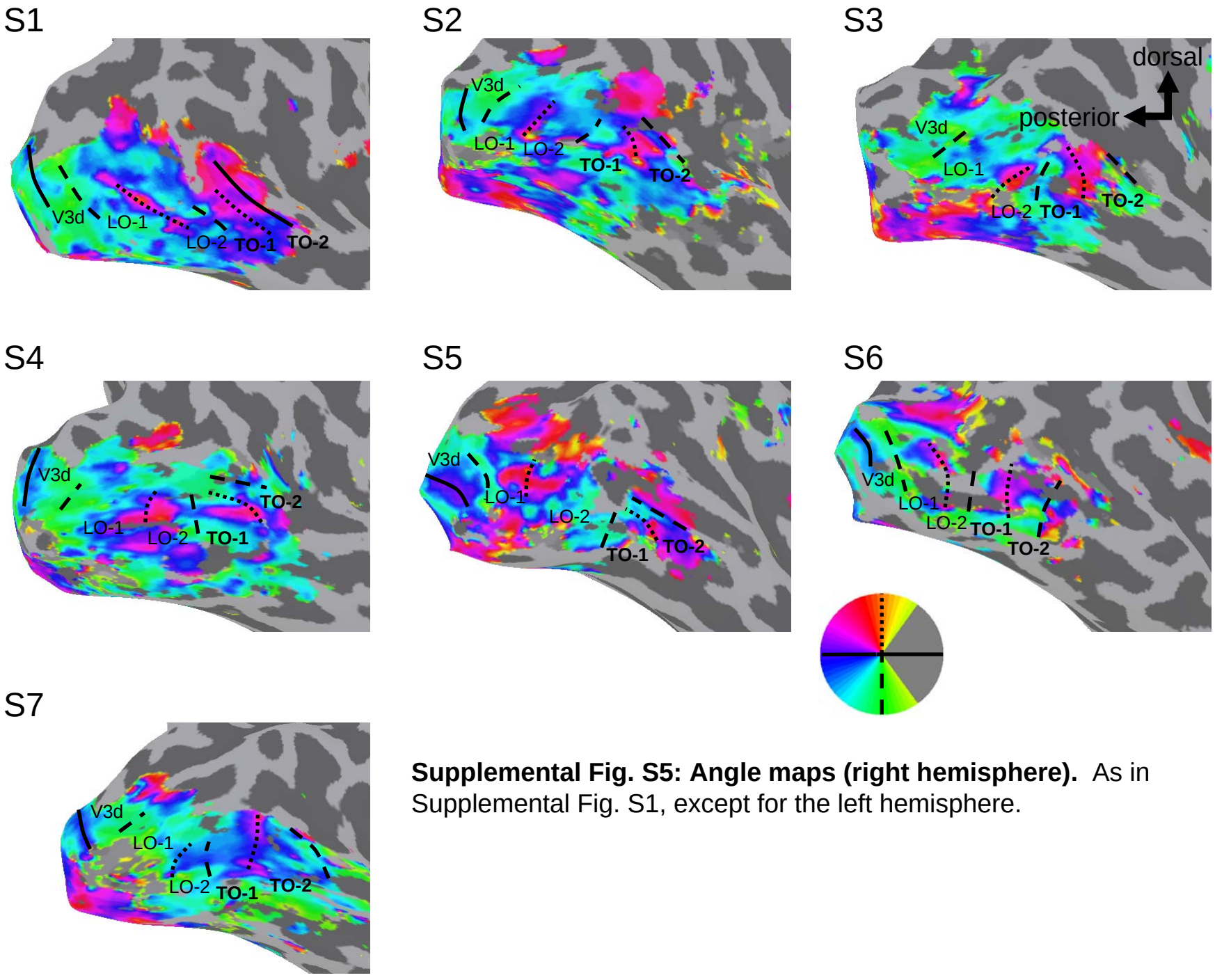

Supplemental Fig. S5: Angle maps (right hemisphere). As in Supplemental Fig. S1, except for the left hemisphere.

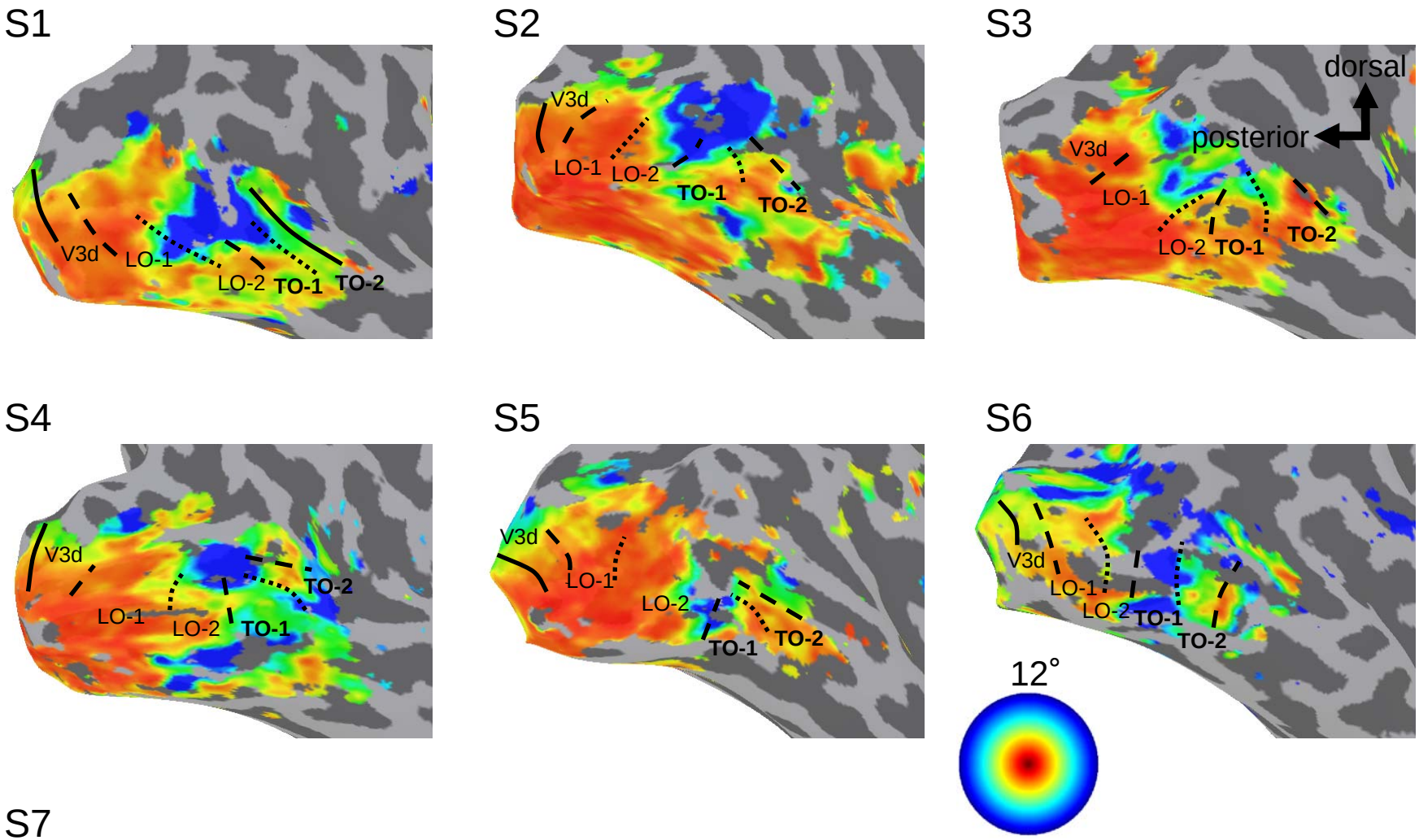

Supplemental Fig. S6: Eccentricity maps of all subjects (right hemisphere). As in Supplemental Fig. S2, except for the left hemisphere.

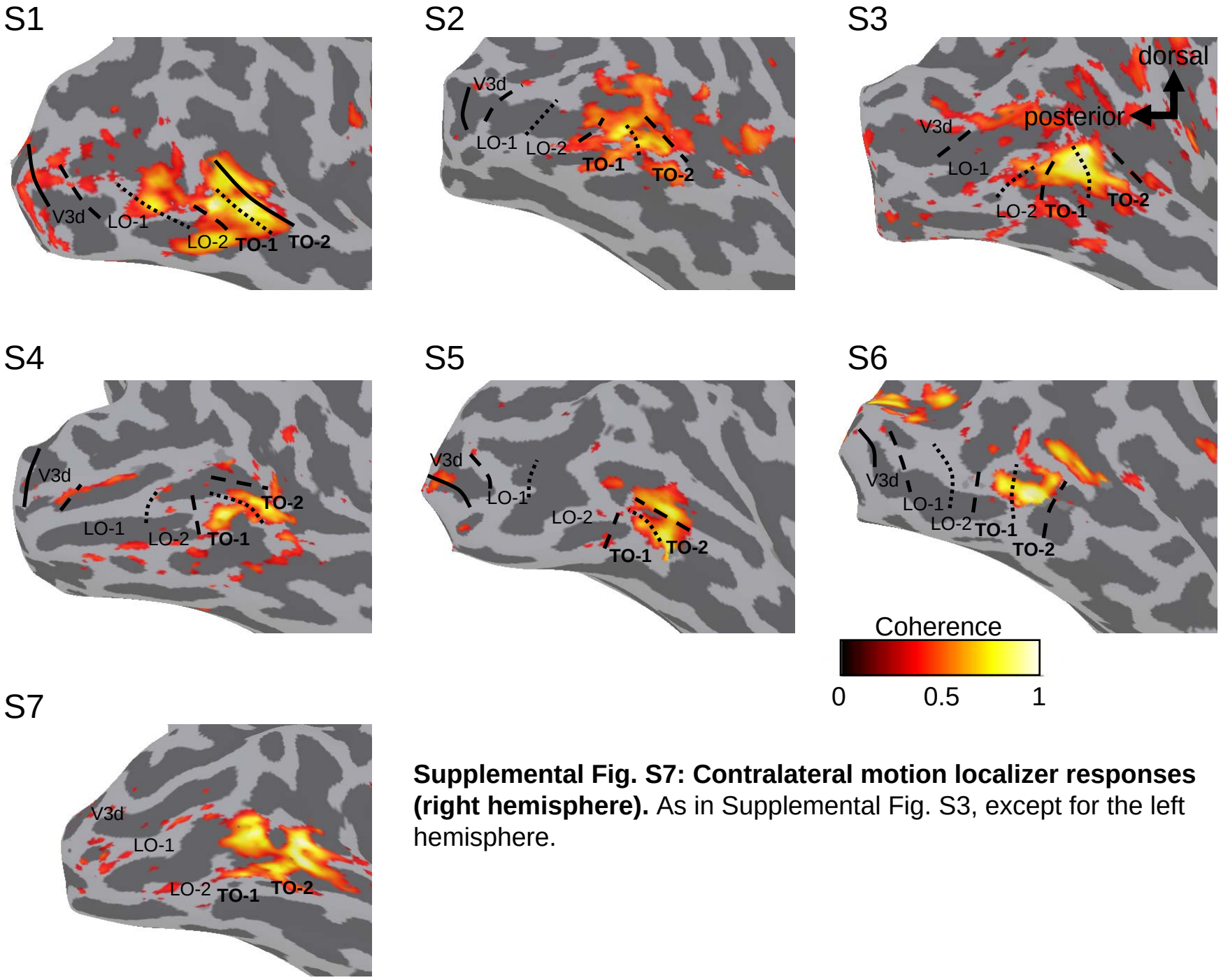

Supplemental Fig. S7: Contralateral motion localizer responses (right hemisphere). As in Supplemental Fig. S3, except for the left hemisphere.

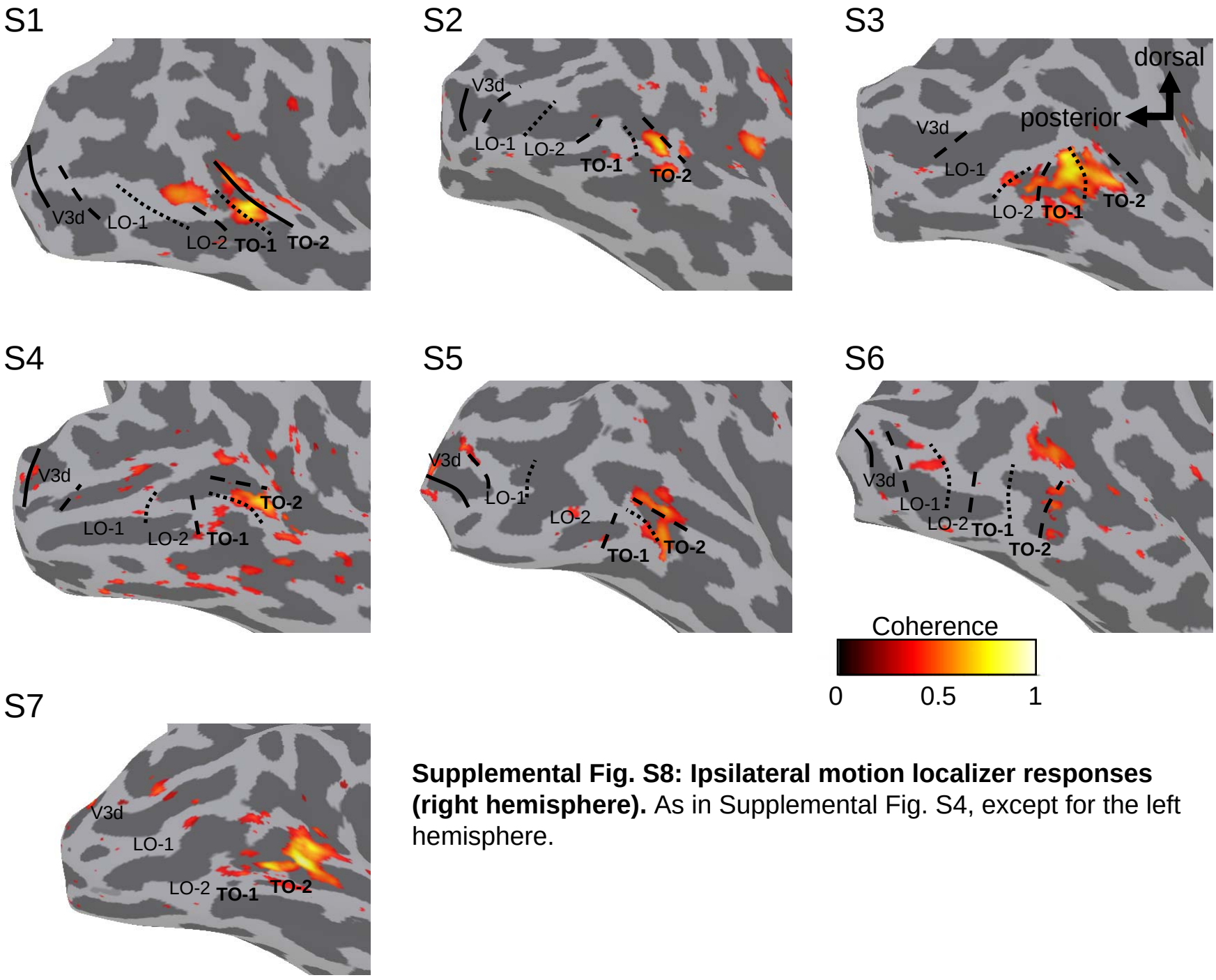

Supplemental Fig. S8: Ipsilateral motion localizer responses (right hemisphere). As in Supplemental Fig. S4, except for the left hemisphere.

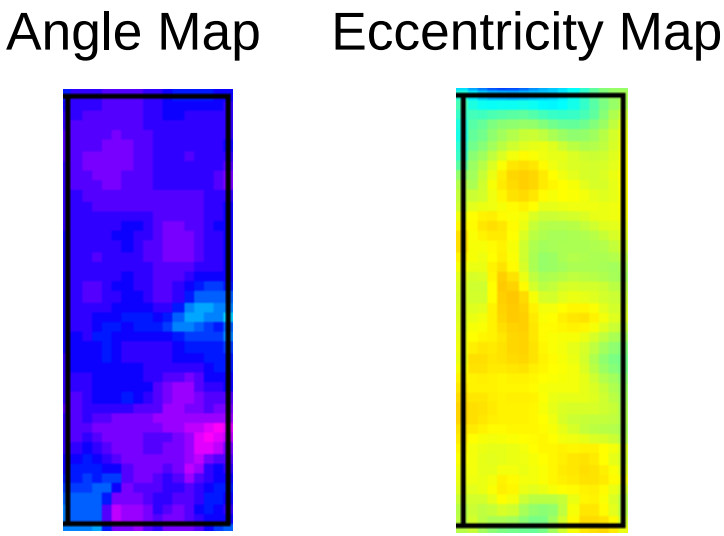

Supplemental Fig. S9: Atlas-based averaging applied to noise adjacent to TO-2. The atlas-based averaging procedure was applied to the data directly abutting and anterior to TO-2. We initiated the non-linear atlas template fit by selecting one edge on TO-2 and the second edge ~1 cm anterior and parallel to this border (same size as TO-2). The derived atlas-based average eccentricity and angle maps are shown. Neither the angle or eccentricity map is regular.

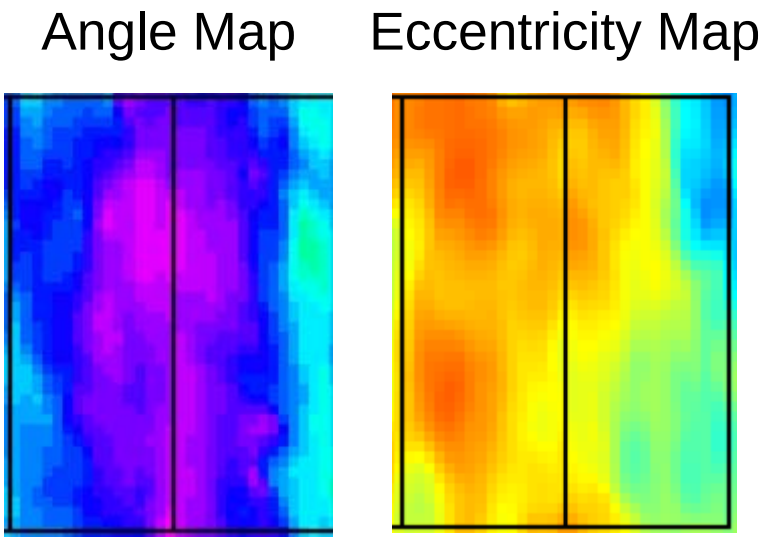

Supplemental Fig. S10: Atlas-based averaging applied to biased noisy data. The atlas-based averaging procedure was applied to the noisy data either superior or inferior to the TO-maps where we could not discern any systematic retinotopic organization. The procedure was biased, however, by initiating the atlas-fitting with two quadrilateral boundaries that fell on upper and lower vertical meridian representations. In this case, we derived an acceptable angle map that reflects the choice of the initial starting positions (left panel). The derived eccentricity map, however, is not regular. Moreover, the derived fit does not have a regular pRF-size map (not shown), or align with localizer responses.

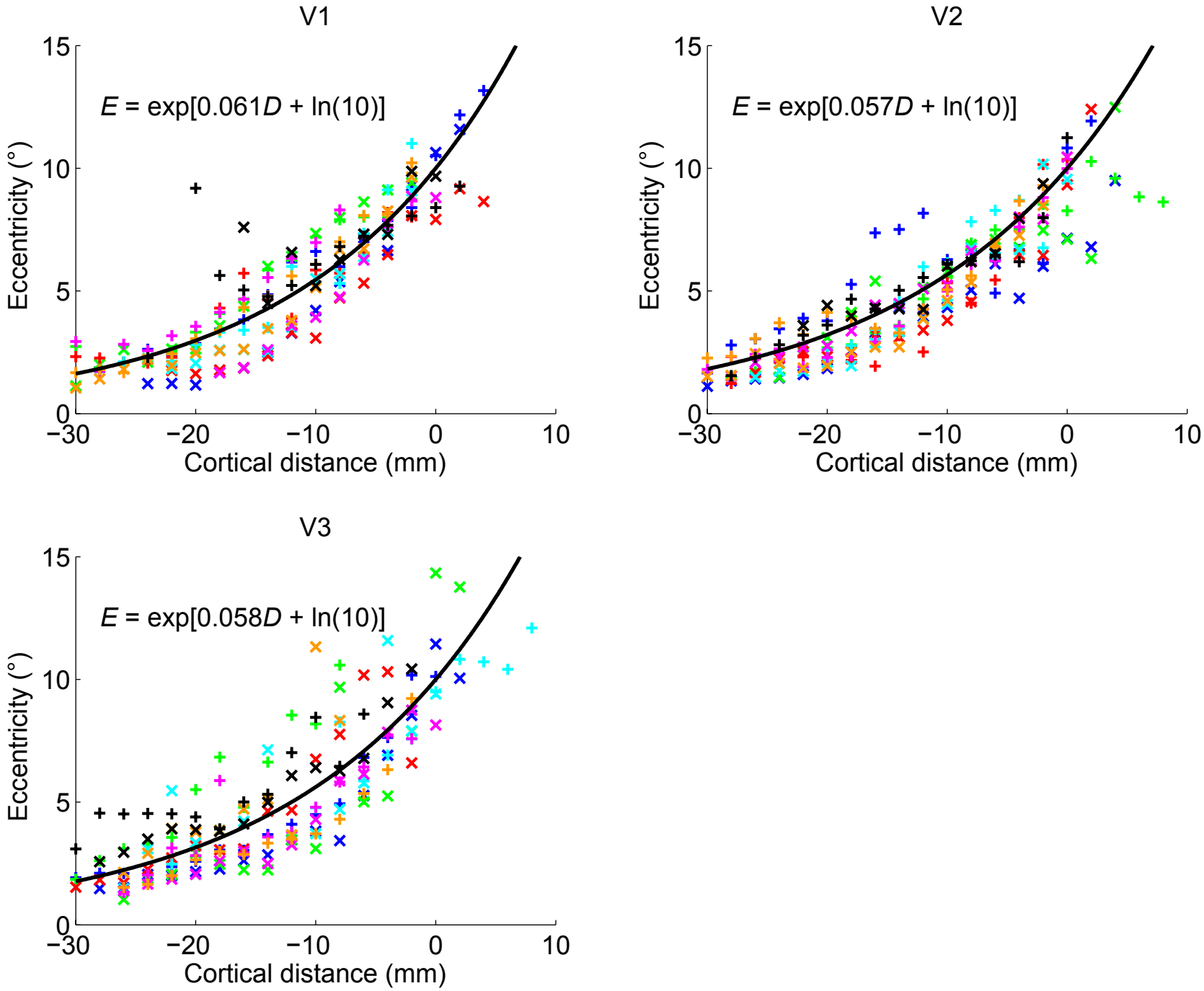

Supplemental Fig. S11: Visual field eccentricity as a function of cortical position for V1-V3. Other aspects as in Fig. 4.

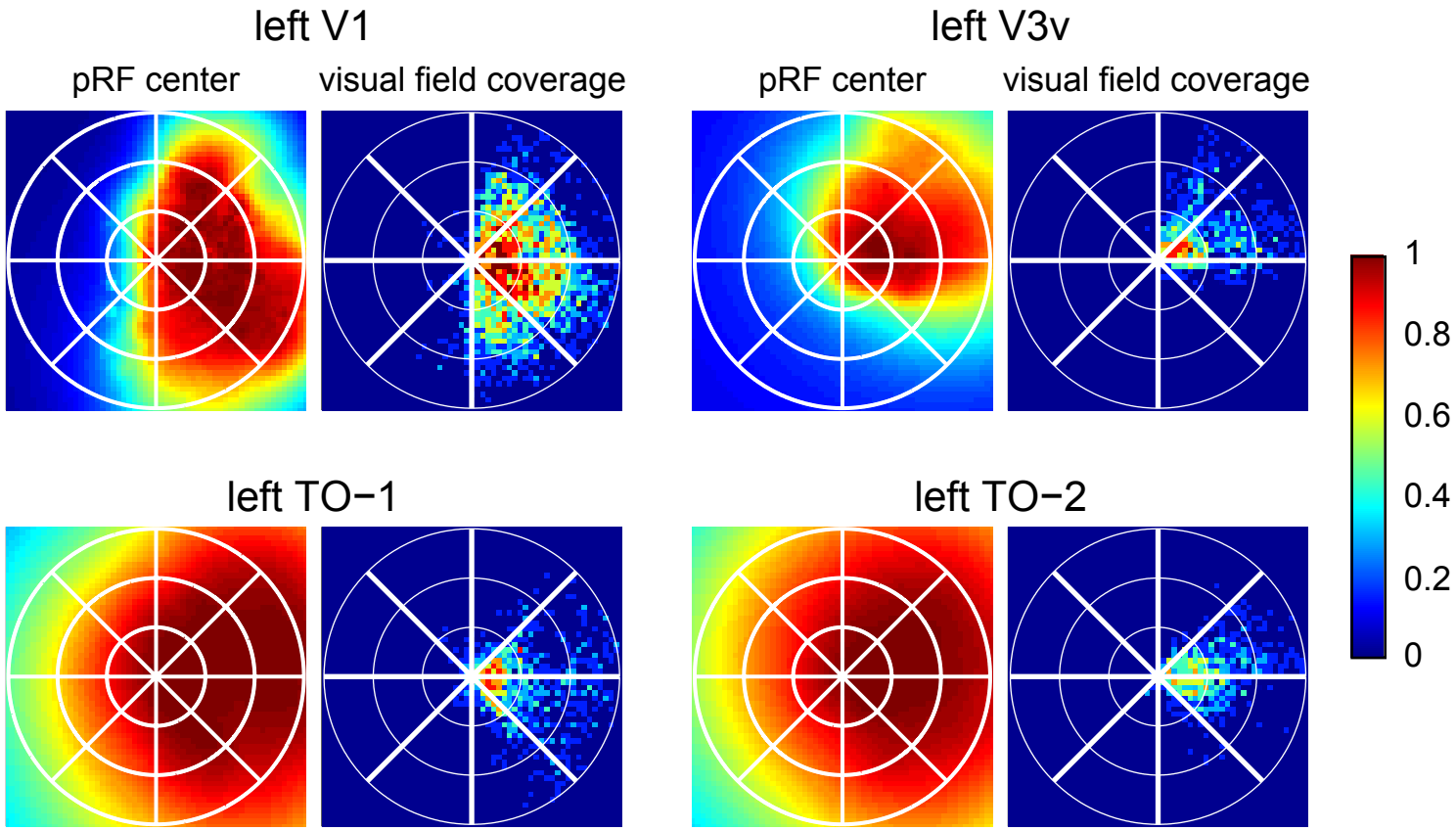

Supplemental Fig. S12: Averaged pRF center distribution and visual field coverage of left hemisphere. The left panels show only the pRF centers; the right panels incorporate the pRF sizes in the computation of the visual field coverage.

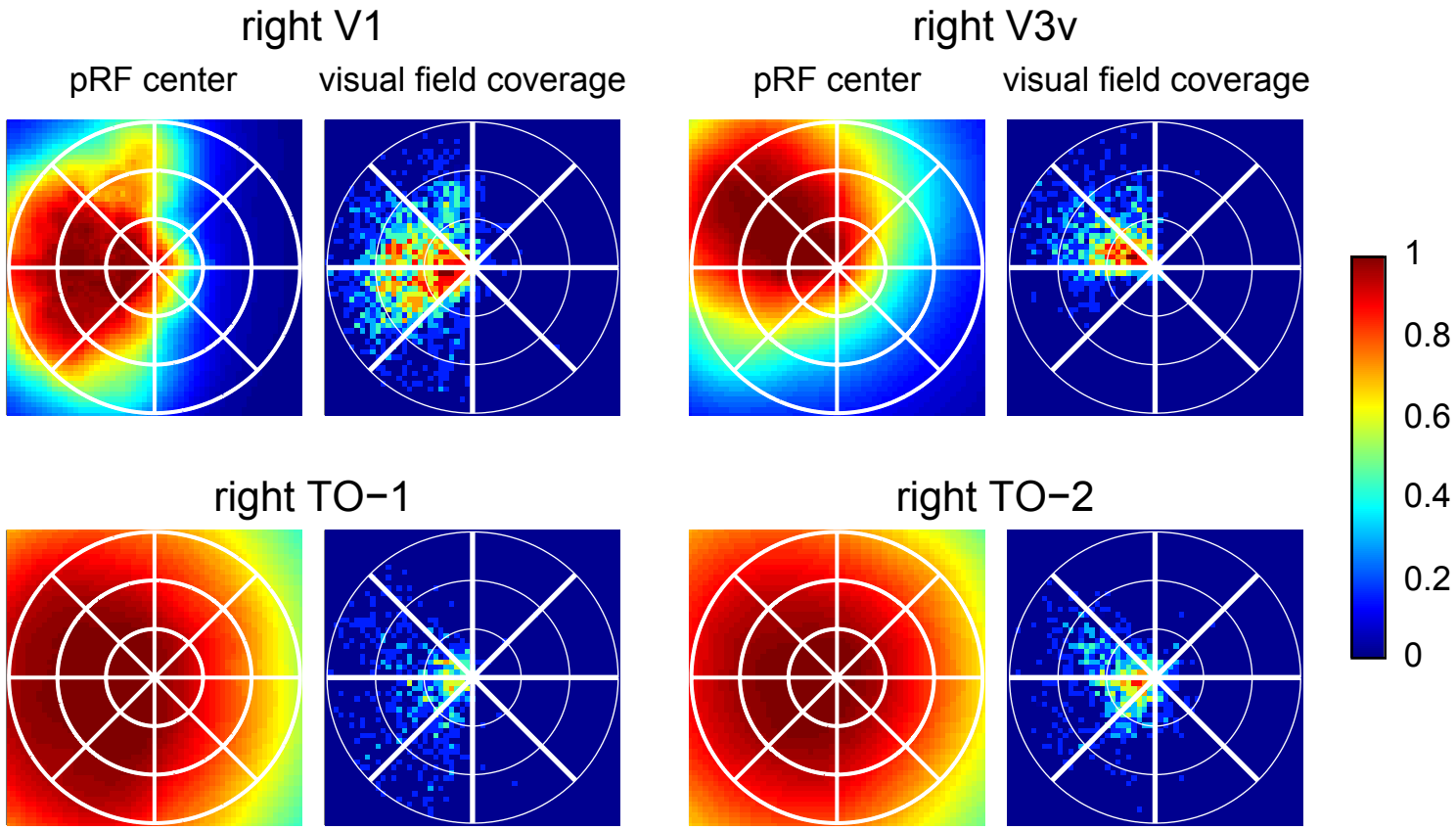

Supplemental Fig. S13: Averaged pRF center distribution and visual field coverage of right hemisphere. The left panels show only the pRF centers; the right panels incorporate the pRF sizes in the computation of the visual field coverage.

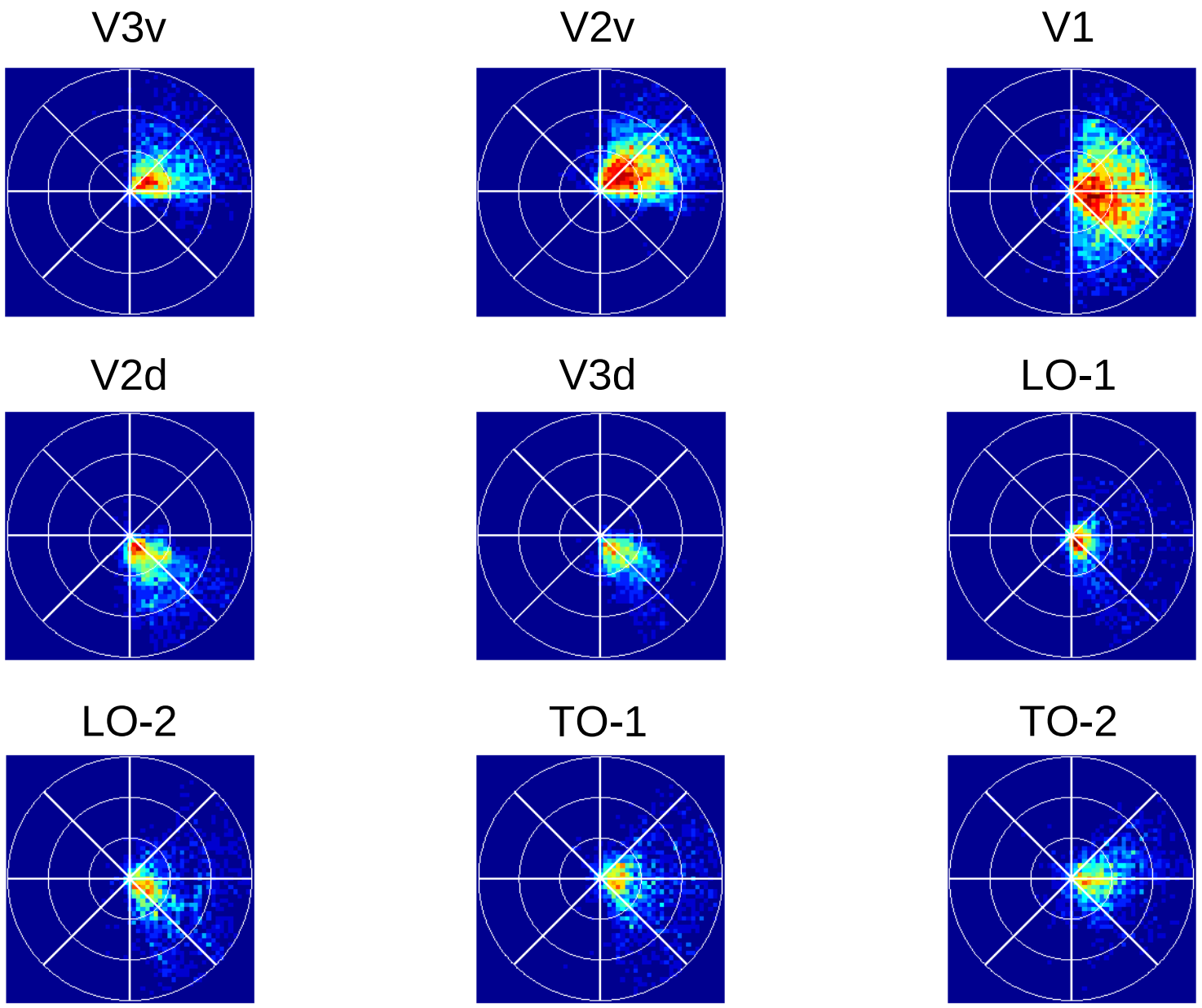

Supplemental Fig. S14: Averaged pRF center distribution of all identified maps. Other aspects as in the left panels of Fig. 7.

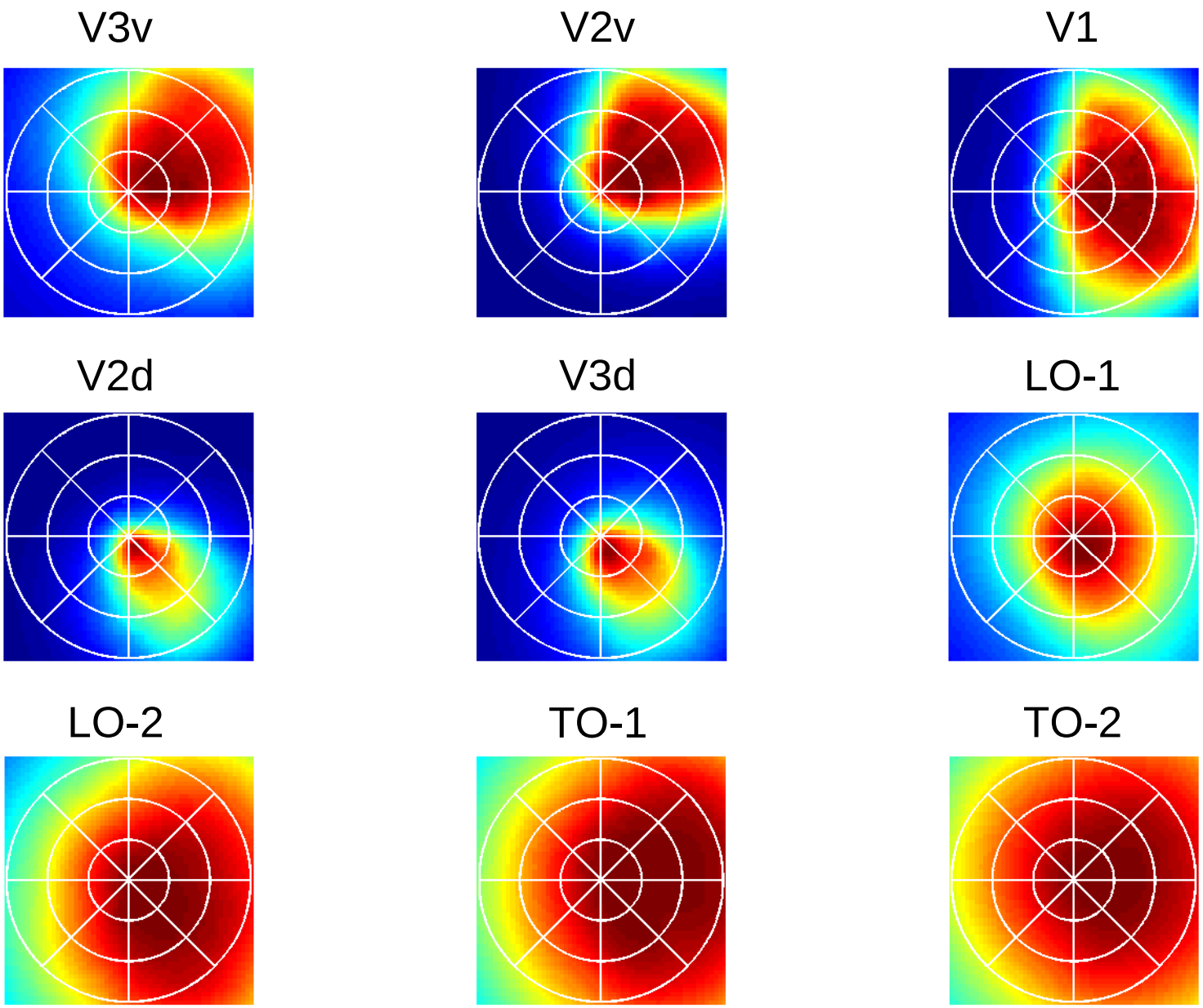

Supplemental Fig. S15: Averaged visual field coverage of all identified maps. Other aspects as in the right panels of Fig. 7.

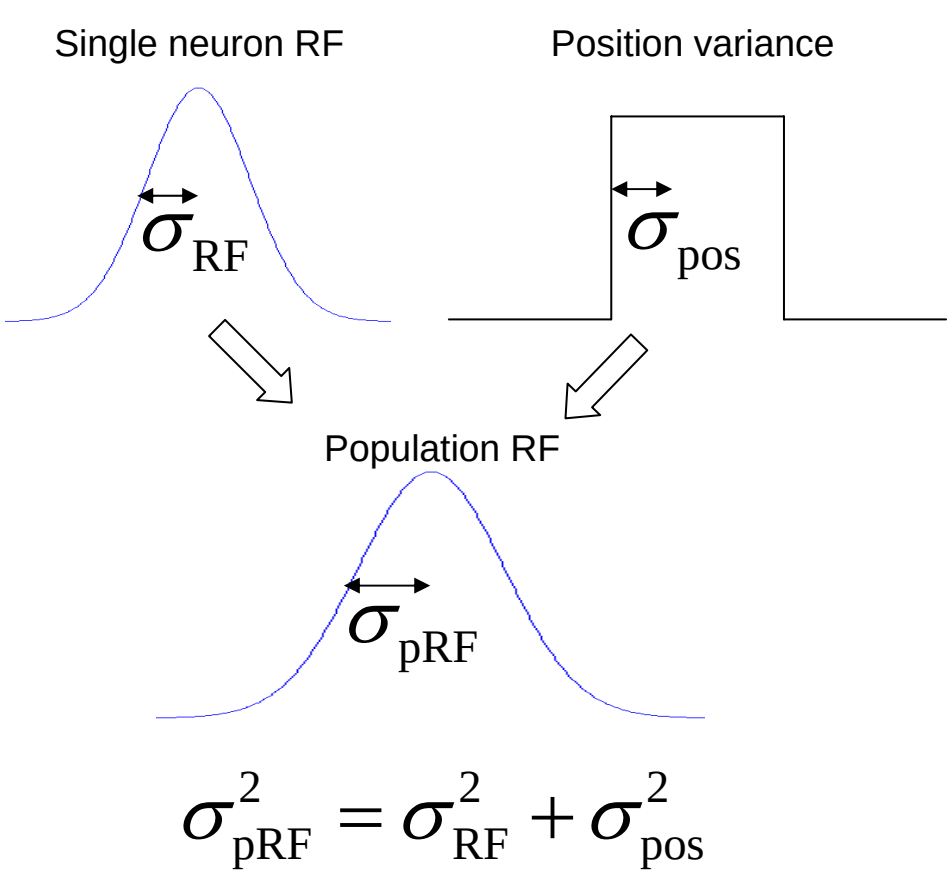

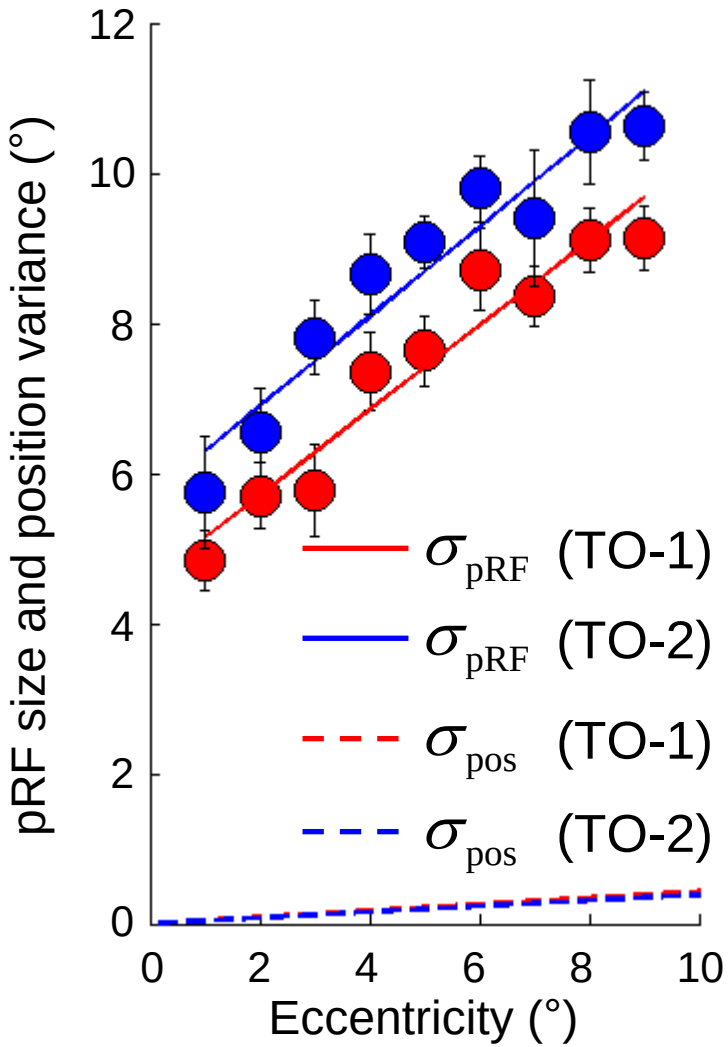

Supplemental Fig. S16: Estimated contribution to measured pRF size from position variance. Position variance within a single voxel depends on the receptive field sizes of neurons contributing to the BOLD signal and the position variance of the centers of these neurons. In theory, these factors contribute additively. We calculated the contribution to the pRF size from the position spread derived from the cortical magnification in the averaged data (Fig. 4). Cortical magnification is the inverse of the slope of the function relating eccentricity to cortical distance. The contribution from position variance is relatively small (< 1°) compared to the measured pRF size (5-10°). The calculation only accounts for variance along the direction of increasing eccentricity; the magnification might be slightly increased if we also included variance from the direction of changing angle. Even so, the estimated pRF size appears to depend mainly on the receptive field sizes of the neurons contributing to the BOLD signal.